with underlying gypsum and minor deposits of carbonates at the base. Kieserite and other K or Mg salts are minor components appearing at the top of the sequence. We can outline the large accumulation of kieserite of the Zechstein basin of the Permian epoch and the deposition of magnesium sulfates in the currently drying Aral Sea.
22. M. A. Bullock *et al.*, *Icarus* **170**, 404 (2004).
23. D. C. Catling, *J. Geophys. Res.* **104**, 16453 (1999).
24. A. G. Fairen *et al.*, *Nature* **431**, 423 (2004).
25. S. W. Squyres *et al.*, *Science* **306**, 1698 (2004).
26. D. L. Huston *et al.*, *Earth Planet. Sci. Lett.* **220**, 41 (2004).
27. R. E. Arvidson *et al.*, *Science* **307**, 1591 (2005); published online 17 February 2005 (10.1126/science.119509).
28. Green *et al.*, *IEEE Trans. Geosc. Rem. Sens.* **26**, 65 (1993).
29. G. R. Hunt *et al.*, *Mod. Geol.* **3**, 1 (1971).
30. J. Bishop, E. Murad, *Am. Miner.*, in press.
31. Laboratory reflectance data provided through a cooperation with NASA and the Compact Reconnaissance Imaging Spectrometer for Mars (CRISM) team. Reflectance measurements were acquired at the Reflectance Experiment Laboratory (RELAB) at Brown University. Efforts to acquire these data by J. F. Mustard are gratefully acknowledged.

12 December 2004; accepted 7 February 2005
Published online 17 February 2005;
10.1126/science.1109087
Include this information when citing this paper.

REPORT

Spectral Reflectance and Morphologic Correlations in Eastern Terra Meridiani, Mars

R. E. Arvidson,[1]* F. Poulet,[2] J.-P. Bibring,[2] M. Wolff,[3] A. Gendrin,[2] R. V. Morris,[4] J. J. Freeman,[1] Y. Langevin,[2] N. Mangold,[2] G. Bellucci[5]

The Mars Express Observatoire pour la Minéralogie, l'Eau, les Glaces, et l'Activité (OMEGA) hyperspectral image data covering eastern Terra Meridiani indicate the ubiquitous presence of molecular water in etched terrain materials that disconformably overlie heavily cratered terrains and underlie the hematite-bearing plains explored by the Opportunity rover. Identification of crystalline water in kieserite ($MgSO_4 \cdot H_2O$) is linked to materials exposed in a valley and plateau to the north of hematite-bearing plains. The mineralogical similarities between the etched terrain deposits examined with OMEGA data and the layered rocks examined by Opportunity imply that the ancient aqueous environments inferred from analyses of the rover data extend over regional scales.

The Mars Express instrument, OMEGA, has acquired hyperspectral imaging data of the martian atmosphere and surface since January 2004 (*1*). In this Report, we summarize analyses of OMEGA data from Orbit 485 over Terra Meridiani, acquired on 7 June 2004 at approximately 09:00 Mars local time and a solar incidence angle of ~46°. This Report complements the work on identification and mapping of high-latitude hydrated sulfate minerals (*2*) and in equatorial to mid-latitude layered deposits (*3*) from OMEGA data. Our focus is the identification of hydrated phases associated with etched terrain materials exposed to the east and north of the hematite-bearing plains that define Meridiani Planum (*4*–*6*).

The geologic setting of Terra Meridiani is among the most complex on Mars and includes exposures of Noachian-aged cratered terrains that have been dissected by channel systems that were carved by water flowing from the southeast to the northwest (*7*) (Fig. 1). After channeling ceased, several hundred meters of layered materials were disconformably deposited onto the dissected cratered terrains. To the north of Terra Meridiani, the deposits were then buried by the southern edge of a dust mantle that peaks in thickness over Terra Arabia (*5*). Subsequent wind erosion then exposed the layered deposits in Terra Meridiani and differentially shaped these materials into a set of domes, ridges, plateaus, and other landforms collectively termed etched terrains (*5*). The hematite-bearing Meridiani Planum surfaces and materials mapped from Mars Global Surveyor (MGS) Thermal Emission Spectra (TES) (*8*) and explored by the Mars Exploration Rover, Opportunity (*9*), are at the top of the stratigraphic section of preserved layered materials. Analyses of rover-based data show that the hematite spherules and associated fragments have been concentrated on the surface as a lag deposit as wind erosion has eroded the weak spherule-bearing, sulfate-rich rocks that underlie the plains (*10*).

OMEGA Orbit 485 data cover portions of the eastern hematite-bearing plains, sections of etched terrains exposed to the east and north of the plains, and extensive areas of dissected and mantled cratered terrains (Fig. 1). Furthermore, the northern exposures of etched terrains include deposits in a valley and plateau oriented to the northwest-southeast and located just to the north of the transition from the hematite-bearing plains to the etched terrains (Figs. 1 and 2). After retrieval of surface Lambert normal albedos (*11*), standard reduction analyses using principal components techniques (*12*) were used to extract spectral endmembers. Extractions focused on the wavelength interval from 1.0 to 2.6 μm because interactive inspection of spectra suggested that this region showed the greatest variety of spectral shapes. Five spectral endmembers (Fig. 3) explain 86% of the variance for plains, etched terrains, and surrounding dark cratered terrains: (i) a "bright etched terrain" spectrum typical of the signatures for etched terrain, (ii) a "dark etched plateau" spectrum representative of darker signatures associated with the northwest-southeast–trending valley and plateau (Figs. 1 and 2), (iii) a "bright plains" spectrum, (iv) a "dark plains" spectrum, and (v) a "dark crater floor" spectrum (located in the cratered terrain).

Between 0.4 and 1.0 μm, each of the five endmembers is characterized by an absorption edge between 0.4 and ~0.6 μm, a slope change near 0.6 μm, a relative reflectance maximum at ~0.75 μm, and a band minimum at longer wavelengths. The position of the minimum ranges from ~0.82 μm (feature A, Fig. 3) for the bright etched terrain spectrum to ~1.0 μm (feature B in Fig. 3) for the dark crater floor endmember. The spectral slope between ~0.6 and ~1.5 μm is steep and positive for the bright etched terrain spectrum and slightly negative for the dark crater floor spectrum. All of these spectral features have been detected in previous observations of Mars made at lower spatial resolution as compared to OMEGA data (~2 km for Orbit 485 data versus ~20 km) (*13*, *14*). The spectral features for the bright etched terrain spectrum are consistent with the presence of Fe^{3+}-bearing minerals, interpreted to be a mixture of nanophase ferric iron and hematite (*15*),

[1]Department of Earth and Planetary Sciences, Washington University, St. Louis, MO 63130, USA. [2]Institut d'Astrophysique Spatiale, Batiment 121, 91405, Orsay Campus, France. [3]Space Science Institute, Boulder, CO 80301, USA. [4]NASA Johnson Space Center, Houston, TX 77058, USA. [5]Istituto Nazionale Di Astrofisica Istituto di Fisica dello Spazio Interplanetario, Via Fosso del Cavaliere, 00133 Rome, Italy.

*To whom correspondence should be addressed. E-mail: arvidson@wunder.wustl.edu

although the minimum for well-crystalline and chemically pure hematite is more typically 0.85 to 0.87 μm (*16*). On the other hand, the dark crater floor spectrum is interpreted to result from the presence of relatively unaltered materials with a thin Fe^{3+}-bearing mineral alteration or dust-rich surface layer. This spectrum clearly shows evidence for the Fe^{2+} electronic transition absorption bands (features B and C at ~1 and 2 μm, respectively, in Fig. 3) that are associated with pyroxene in basaltic materials (*17*).

The bright plains spectral endmember, on the basis of examination of MGS Mars Orbital Camera and Odyssey Thermal Emission Imaging System (THEMIS) image data, shows that the material represented by this endmember is located where hematite-bearing, mottled plains dominate the surface. In some locations, layering is exposed along relatively steep slopes. Additionally, the bright plains spectrum has a similar shape but lower overall reflectance as compared with the bright etched terrain endmember (Fig. 3). We interpret the spectral similarity between bright plains and etched terrain endmembers, and the appearance of the bright plains, as indicative of wind erosion and exposure of some etched terrain material in these areas, with a partial cover of hematite-bearing spherules and basaltic sands similar to what was found at the Opportunity site several hundred kilometers to the southwest (*18*). The partial cover subdues the water-related spectral features typical of well-exposed etched terrains. The dark plains endmember is spectrally flat from ~1.3 to 2.6 μm and is representative of the spectral signatures for slightly rolling, smooth plains with homogeneous brightness. Bowl-shaped craters are present and well preserved. No exposed layering is evident. These dark plains are interpreted to be covered with an areally uniform dark lag deposit of hematite spherules and basalt sands formed as the plains were slowly eroded by wind. Based on mapping the areal abundance of hematite from TES data (*5*), the bright and dark plains imaged by OMEGA during Orbit 485 have higher basalt sand–to–hematite spherule abundances as compared with the plains examined by Opportunity.

The deep band at ~3 μm in all spectra (feature D in Fig. 3) results from the well-known stretching fundamental vibrations of the H_2O molecule (ν_1 and ν_3) (*19*). This feature has been previously detected, including over Terra Meridiani (*20*). It is estimated that <4% water is needed to produce the magnitude of the observed absorptions for Mars (*21*), although the enhanced depths for the bright etched terrain as compared with those of other regions suggest a larger number. The feature at 1.92 μm (feature E in Fig. 3) is well expressed in the spectra for bright etched terrain and is diagnostic of the presence of the H_2O molecule and results from combination of two fundamental vibrations ($\nu_2 + \nu_3$) (*19*). In the absence of spectral evidence for hydrated and hydroxolated phases in the spectrum, we associate feature E with water adsorbed onto surface materials. The strength of the ~3- and 1.92-μm features for etched terrain spectra implies that materials exposed in these deposits are enhanced in their water contents relative to the other units for which spectral endmembers were extracted. A spectral feature near 1.4 μm should also be present for these water-bearing materials but is not apparent (Fig. 3), presumably because it is too weak to be observed in the retrieved reflectance data.

The last three spectral features, corresponding to F (~2.5 μm) in the bright etched terrain spectrum and to G (~2.1 μm) and H (~2.4 μm) in the dark etched plateau spectrum, require additional analyses before assignments can be made. Each spectrum was normalized to the endmember spectrum for the dark plains for the 1.6- to 2.6-μm region. The dark plains spectrum is flat in this wavelength interval and thus provides a reason-

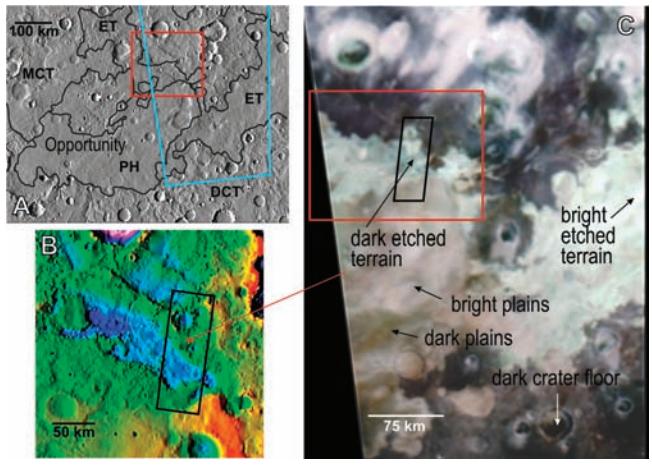

Fig. 1. (**A**) Shaded relief map of Meridiani Planum region showing the dissected cratered terrain (DCT) disconformably overlain by etched terrain deposits (ET), which in turn are covered by hematite-bearing plains (PH). To the north, the deposits are mantled by younger deposits (MCT). The Opportunity landing site is shown, along with boxes that delineate an enlarged portion of the shaded relief map (red) shown in (**B**) and coverage for Orbit 485 OMEGA data (blue) shown in (**C**). Units are updated from (*5*). Topographic information is from MGS Mars Orbital Laser Altimeter (MOLA) data (*27*). Simulated sun is from west with an angle of 15° above horizon. (**B**) Shaded relief map shown in (A) with color-coded elevations overlain and location of THEMIS image subframe (C) denoted by black box. Elevation ranges from a high of –690 m (red) to a low of –1750 m (purple) relative to the International Astronomical Union–2000 coordinate system and MOLA-based areoid. (**C**) OMEGA false-color infrared composite (band wavelengths 1.2992, 1.7576, and 2.3947 μm as blue, green, and red, respectively) covering eastern Terra Meridiani with locations of shaded relief map and THEMIS coverage [(A) and (B)] shown as red and black boxes, respectively. Locations for which OMEGA spectra endmember spectra were extracted are also shown.

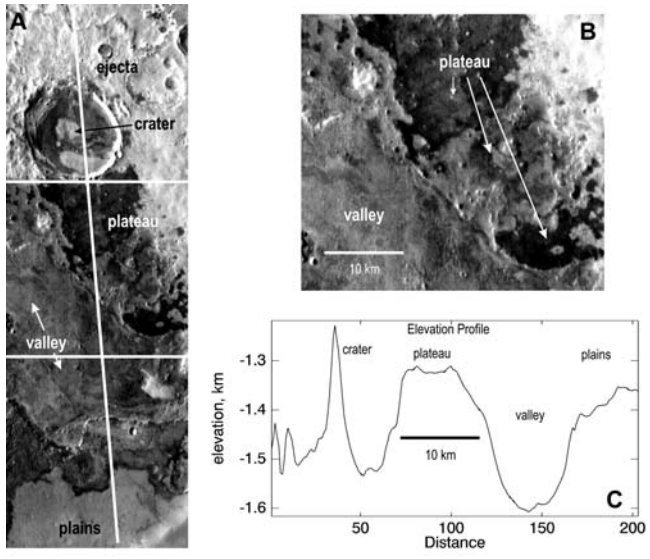

Fig. 2. (**A**) THEMIS scaled daytime infrared image subframe showing major geomorphic units including etched terrain materials exposed on a plateau and in a valley. White line shows location of vertical profile shown in (C). Image ID: I02434005BTR.img acquired on 2 July 2002 at ~16:00 Mars local time. Regions covered in the image all have elevated and similar thermal inertias (*5*). Thus, the overall reflectance in the visible and reflected infrared controls the afternoon temperature. Warm surfaces (high brightness) in the THEMIS data correspond to the dark (and thus absorbing in solar wavelengths) regions in the OMEGA data shown in Fig. 1C. (**B**) Enlarged view of portion of THEMIS subframe showing the valley and plateau. The dark etched endmember was derived from the plateau region. (**C**) Vertical topographic profile from MOLA data (128 pixels/degree bins) with 100 times vertical exaggeration.

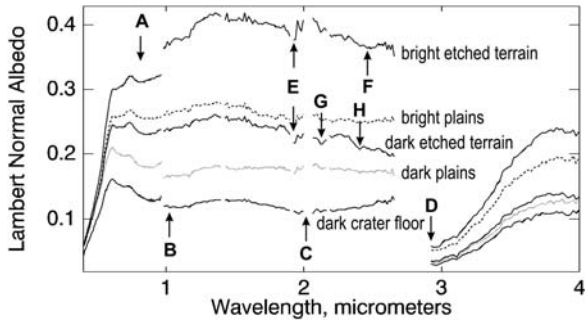

Fig. 3. OMEGA-based reflectance spectra for spectral endmember units with letters to denote spectral features. Gaps correspond to wavelengths with channels exhibiting anomalous behavior or not properly modeled with our radiative transfer techniques. The vertical offsets at ~1 μm for some spectra are associated with residual calibration errors.

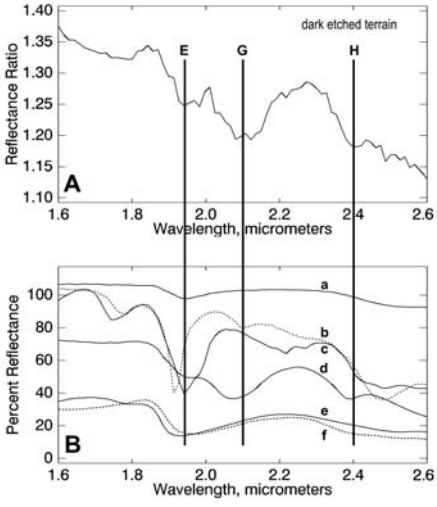

Fig. 4. (**A**) OMEGA-based reflectance spectrum for dark etched plateau region divided by the spectrum for dark plains and compared in (**B**) with laboratory spectra for various sulfate minerals. Minerals: a, barite ($BaSO_4$ with a trace amount of water); b, bassanite ($CaSO_4 \cdot 0.5H_2O$); c, gypsum ($CaSO_4 \cdot 2H_2O$); d, kieserite ($MgSO_4 \cdot H_2O$); e, calcium fluoride (CaF_2) mixed with a small amount of water to simulate water adsorbed on mineral surfaces; and f, epsomite ($MgSO_4 \cdot 7H_2O$). For each sample, sand-sized particles were run in a diffuse reflectance mode in a Nicolet 670 Fourier Transform Spectrometer system fitted with KBr optics, HgCdTe-B detector, and Harrick Cricket (TM) reflectance accessory. Reflectance is expressed relative to a diffuse gold surface.

able spectrum for normalization. The reason for the normalization is to minimize artifacts resulting from imperfect instrument calibration and atmospheric removal. The ratio spectrum enhances the depths of these features G and H and the 1.92-μm H_2O feature (Fig. 4). The ratio spectrum was compared with a number of laboratory-based reflectance spectra of a range of minerals, focusing on sulfate-bearing minerals that have water of crystallization after reconnaissance comparisons suggested that hydrated sulfates provide the best matches (Fig. 4). The bands at ~2.1 and ~2.4 μm, which are interpreted to be combination bands involving the stretching vibration of H_2O molecules within a crystal lattice, best match our laboratory spectrum of kieserite ($MgSO_4 \cdot H_2O$; Fig. 4). The spectrum of the monohydrate of ferrous sulfate (szomolnokite) is similar in this region, but the presence of the mineral is not indicated because its ferrous band minima near 0.94 and 1.33 μm and reflectance maximum near 0.67 μm (*22*, *23*) are not evident in OMEGA spectra. A similar ratio operation for the bright etched terrain spectrum produced a strong band (feature E) consistent with the presence of adsorbed molecular water as discussed above. The identification of H_2O-bearing minerals in the etched terrains, and the presence of kieserite for the valley and plateau, does not mean that the relevant materials are composed only of these phases. Rather, these mineral phases are present in relatively high abundances relative to other areas we examined in this paper. On the basis of our analyses, etched units are also enriched in Fe^{3+}-bearing minerals. In addition, modeling of TES spectral emissivity data suggests that pyroxene, plagioclase feldspar, and glass are also present in etched terrain deposits (*5*).

Comparison of OMEGA and THEMIS data shows that the dark etched plateau region with the kieserite signature is located between two deposits of the more typical bright etched terrain (Fig. 2). Furthermore, the kieserite-bearing surface exhibits a set of domes that is not typical of the rest of the valley and plateau system (Fig. 2). These domes also appear in the valley on the left-hand edge of the THEMIS frame shown in Fig. 2, exactly where OMEGA data also show a spectrum indicative of kieserite. Perhaps the domes evident in the valley and plateau and associated with a kieserite signature are preserved eruptive volcanic cones that were buried, altered by corrosive ground water, and then exhumed by wind. Alternatively, the domes could be a consequence of preferential cementation of materials by ground water preferentially flowing along fractures. Subsequent wind erosion may have left these regions as local domes because of their indurated nature. Examination of THEMIS data for all the etched terrains evident in Orbit 485 suggests that preferential cementation along fractures, followed by differential erosion to produce ridges and plateaus, was a common occurrence (*24*).

The most important conclusion of this paper is that the etched terrain layered materials exhibit evidence for molecular water adsorbed onto the surface materials and, for the dark etched plateau, incorporated as structural water in the hydrated sulfate mineral kieserite. These results complement the analyses conducted by the Opportunity rover on the bright layered rocks in Eagle and Endurance craters, where evidence for hydrated sulfate minerals was also found, including kieserite (*25*). It is our conclusion that Opportunity examined the upper section of the etched terrain deposits in these craters and that our results imply that aqueous processes were involved in forming and/or altering the etched terrain materials over distances of hundreds of kilometers and throughout the several-hundred-meter thickness of the etched terrain deposits.

References and Notes

1. J.-P. Bibring *et al.*, *Science* **307**, 1576 (2005); published online 17 February 2005 (10.1126/science.1108806).
2. Y. Langevin *et al.*, *Science* **307**, 1584 (2005); published online 17 February 2005 (10.1126/science.1109091).
3. A. Gendrin *et al.*, *Science* **307**, 1587 (2005); published online 17 February 2005 (10.1126/science.1109087).
4. B. M. Hynek *et al.*, *J. Geophys. Res.* **107**, 5088, 10.1029/2002JE001891 (2002).
5. R. E. Arvidson *et al.*, *J. Geophys. Res.* **108**, 8073, 10.1029/2002JE002041 (2003).
6. B. M. Hynek, *Nature* **431**, 156 (2004).
7. B. M. Hynek, R. J. Phillips, *Geology* **29**, 407 (2001).
8. P. R. Christensen *et al.*, *J. Geophys. Res.* **105**, 9623, 10.1029/1999JE001093 (2000).
9. S. W. Squyres *et al.*, *Science* **306**, 1698 (2004).
10. R. E. Arvidson *et al.*, *Science* **306**, 1730 (2004).
11. OMEGA data for Orbit 485 over Terra Meridiani were reduced to Lambert normal albedos for each of the 352 wavelengths through the use of a multiple scattering code that models atmospheric aerosol (and Rayleigh) scattering and molecular absorption (*26*) with atmospheric parameters derived from Opportunity and TES data acquired close in time to data for Orbit 485. For wavelengths longer than 2.5 μm, additional terms in the model included thermal emission of the surface and atmosphere. Examination of surface reflectance retrievals demonstrates that atmospheric features are properly modeled and/or the radiometric calibrations for the instrument are well understood for all but the longest wavelengths in the OMEGA data (4.00 to 5.08 μm). Consequently, OMEGA data from this wavelength interval are not discussed in this Report.
12. A. A. Green *et al.*, *IEEE Trans. Geosci. Remote Sensing* **26**, 65 (1988).
13. J. F. Mustard, J. F. Bell III, *Geophys. Res. Lett.* **21**, 353 (1994).
14. S. Murchie *et al.*, *Icarus* **147**, 444 (2000).
15. R. V. Morris *et al.*, *J. Geophys. Res.* **105**, 1757 (2000).
16. R. V. Morris *et al.*, *J. Geophys. Res.* **90**, 3126 (1985).
17. J. F. Mustard *et al.*, *Science* **307**, 1594 (2005); published online 17 February 2005 (10.1126/science.1109098).
18. J. F. Bell *et al.*, *Science* **306**, 1703 (2004).
19. G. Herzberg, *Molecular Spectra and Molecular Structure* (Van Nostrand Reinhold Company, New York, 1945).
20. A. M. Baldridge, W. M. Calvin, *J. Geophys. Res.* **109**, E04S90, 10.1029/2003JE002066 (2004).
21. A. S. Yen *et al.*, *J. Geophys. Res.* **103**, 11125 (1998).
22. J. K. Crowley *et al.*, *Geochem. Explor. Environ. Anal.* **3**, 219 (2003).
23. J. L. Bishop *et al.*, in preparation.
24. For an example, see THEMIS image V03445003, which shows areas within the eastern etched terrain exhibit a polygonal ground pattern. In places, the polygons have been eroded to expose interconnected ridges consisting of materials emplaced within the valleys separating the polygons.
25. P. R. Christensen *et al.*, *Science* **306**, 1733 (2004).

26. K. Stamnes *et al.*, *Appl. Opt.* **27**, 2502 (1988).
27. D. E. Smith *et al.*, *J. Geophys. Res.* **106**, 23689, 10.1029/2000JE001364 (2001).
28. R.E.A., M.W., and R.V.M. acknowledge NASA support for this work. We thank the personnel involved in acquisition and reduction of Mars Express OMEGA data for their efforts. We also thank M. Lane and J. Bishop for reviews of this Report.

7 January 2005; accepted 4 February 2005
Published online 17 February 2005;
10.1126/science.1109509
Include this information when citing this paper.

REPORT

Olivine and Pyroxene Diversity in the Crust of Mars

J. F. Mustard,[1]* F. Poulet,[2] A. Gendrin,[2] J.-P. Bibring,[2] Y. Langevin,[2] B. Gondet,[2] N. Mangold,[3] G. Bellucci,[4] F. Altieri[4]

Data from the Observatoire pour la Minéralogie, l'Eau, les Glaces, et l'Activité (OMEGA) on the Mars Express spacecraft identify the distinct mafic, rock-forming minerals olivine, low-calcium pyroxene (LCP), and high-calcium pyroxene (HCP) on the surface of Mars. Olivine- and HCP-rich regions are found in deposits that span the age range of geologic units. However, LCP-rich regions are found only in the ancient Noachian-aged units, which suggests that melts for these deposits were derived from a mantle depleted in aluminum and calcium. Extended dark regions in the northern plains exhibit no evidence of strong mafic absorptions or absorptions due to hydrated materials.

The igneous composition of the martian crust has been examined through remotely sensed data, meteorites, and in situ observations by landers and rovers (*1*). Meteorites exhibit the greatest petrologic diversity but are, with the exception of one sample, <1.3 billion years in age and thus young. Remotely sensed and landed measurements imply that, where exposed, the igneous crust is dominantly basaltic, composed mostly of feldspar and pyroxene (*2*, *3*). Two major divisions in crustal composition are recognized on the basis of their thermal infrared (IR) spectral signatures (*2*). Type I material, predominantly in the equatorial highlands, is basaltic. Type II, found predominantly in the northern lowland plains, has been interpreted to be andesite or basaltic andesite (*4*) as altered basalt with a large component of hydrolytic weathering materials (*5*, *6*), oxidized basalt (*7*), or silica-coated basalt (*8*). There have been a few outcrops of ancient crust identified in thermal emission data that exhibit concentrations of olivine (*9*) and low-calcium pyroxene (LCP) above the limits of detection (*10*).

Here, we present the first results for the crustal composition of Mars derived from the OMEGA reflectance observations. Visible/near-infrared (NIR) reflectance measurements are most sensitive to the presence of iron-bearing mafic minerals. These analyses complement existing observations, help to resolve issues, and provide insight into the crustal composition and evolution.

The OMEGA experiment and operations are described elsewhere (*11*, *12*). This analysis focuses on visible/NIR reflectance measurements of OMEGA (0.35 to 2.6 μm), where observations of surface reflectance also include atmospheric contributions from dust, water ice aerosols, CO_2, and H_2O vapor. We perform an atmospheric correction assuming that the surface and atmospheric contributions are multiplicative and that the atmospheric contribution follows a power law variation with altitude (*13*). An atmospheric spectrum is derived from a high-resolution observation crossing the summit of Olympus Mons. Assuming a constant surface contribution, the ratio of a spectrum from the base of Olympus Mons to one over the summit provides the atmospheric spectrum at a power function of their difference in altitude. The atmospheric contribution to each spectrum is then removed by dividing the observation by the derived atmospheric spectrum, scaled by the strength of the CO_2 atmospheric absorption measured in the observation.

Olivine and pyroxene are two important classes of rock-forming minerals that have absorption bands in the visible/NIR that result from electronic crystal field transitions of Fe in octahedral coordination (*14*). These absorptions are diagnostic of the minerals and their chemical composition (*15*, *16*). Olivine [$(Mg,Fe)_2SiO_4$] has a broad, complex absorption centered near 1 μm that varies in width, position, and shape with increasing Fe content (*16*). Pyroxenes [$(Ca,Fe,Mg)_2Si_2O_6$] are recognized by the presence of two distinct absorptions centered near 1 and 2 μm, where the band centers shift toward longer wavelengths with increasing calcium content. LCPs (e.g., orthopyroxene) have short-wavelength band centers (0.9 and 1.8 μm), whereas high-calcium pyroxenes (HCPs) (e.g., clinopyroxene) typically have long-wavelength band centers (1.05 and 2.3 μm) (*15*). Laboratory measurements of these minerals and their mixtures (*15*–*18*) provide the basis for interpreting the OMEGA reflectance spectra.

The detection of specific minerals from reflectance spectra involves several steps. First the atmospherically corrected data must demonstrate the presence of unique spectral features that exceed the noise or any systematic variations of the measurements. Typically, the spectral features are weak because of mixing with bright dust on Mars. In addition, there may be residual atmospheric or instrumental effects that affect the shape and strength of diagnostic absorptions and, thus, mineral interpretation. To enhance the spectral features of the important material, we find the ratio of the observed spectrum to that of a nearby dusty region with a similar atmospheric path length acquired during the same observation sequence. Spectra of bright dust exhibit no mafic mineral features, and this dust is a product of alteration processes (i.e., not fine-grained or powdered crustal material). Thus, spectral properties that are common between the measurements, including residual atmospheric effects, cancel out, leaving in the ratio the spectral properties of the material of interest. In the mineral identifications presented here, we show the original OMEGA spectra of the target terrain and nearby dusty terrain, with atmospheric correction, the ratio of target terrain to dusty terrain, and candidate spectra of minerals measured in the laboratory.

The detection of olivine is made on the basis of a broad complex of overlapping absorptions centered near 1 μm. The spectrum of the olivine-bearing surface shown in Fig. 1 exhibits a broad and strong absorption between 0.8 and 1.5 μm but is relatively featureless for wavelengths >1.5 μm. This is

[1]Geological Sciences, Brown University, Providence, RI 02912, USA. [2]Institut d'Astrophysique Spatiale, Bâtiment 121, 91405 Orsay Campus, France. [3]IDES, Bâtiment 509, 91405 Orsay Campus, France. [4]IFSI-INAF, Rome, Italy.

*To whom correspondence should be addressed. E-mail: john_mustard@brown.edu